Letter

Tomer Lewi*, Nikita A. Butakov and Jon A. Schuller

Thermal tuning capabilities of semiconductor metasurface resonators

https://doi.org/10.1515/nanoph-2018-0178
Received October 21, 2018; revised November 13, 2018; accepted November 15, 2018

Abstract: Metasurfaces exploit optical phase, amplitude, and polarization engineering at subwavelength dimensions to achieve unprecedented control of light. The realization of all dielectric metasurfaces has led to low-loss flat optical elements with functionalities that cannot be achieved with metal elements. However, to reach their ultimate potential, metasurfaces must move beyond static operation and incorporate active tunability and reconfigurable functions. The central challenge is achieving large tunability in subwavelength resonator elements, which requires large optical effects in response to external stimuli. Here we study the thermal tunability of high-index silicon and germanium semiconductor resonators over a large temperature range. We demonstrate thermal tuning of Mie resonances due to the normal positive thermo-optic effect ($dn/dT > 0$) over a wide infrared range. We show that at higher temperatures and longer wavelengths, the sign of the thermo-optic coefficient is reversed, culminating in a negative induced index due to thermal excitation of free carriers. We also demonstrate the tuning of high-order Mie resonances by several linewidths with a temperature swing of $\Delta T < 100$ K. Finally, we exploit the large near-infrared thermo-optic coefficient in Si metasurfaces to realize optical switching and tunable metafilters.

Keywords: reconfigurable metasurfaces; tunable metasurfaces; thermal tuning; Mie resonators; nanoparticles.

***Corresponding author: Tomer Lewi,** Department of Electrical and Computer Engineering, University of California Santa Barbara, Santa Barbara, CA 93106, USA; and Electrical Engineering, Faculty of Engineering and the Institute for Nanotechnology and Advanced Materials, Bar-Ilan University, Ramat-Gan 5290002, Israel, e-mail: tomer.lewi@biu.ac.il. https://orcid.org/0000-0002-7321-876X
Nikita A. Butakov and Jon A. Schuller: Department of Electrical and Computer Engineering, University of California Santa Barbara, Santa Barbara, CA 93106, USA

1 Introduction

Metasurfaces are planar optical structures composed of ordered subwavelength resonators, designed to manipulate light through arbitrary wavefront shaping [1–4]. Recently, this field has witnessed tremendous progress by adopting an all-dielectric approach [2], giving rise to several dielectric metasurface demonstrations, including achromatic and broadband metalenses [5–7], axicon lenses [8], sub-diffraction focusing [9], nonlinear generation [10–12], beam deflectors [8, 13, 14], wave plates and beam converters [15–18], holograms [19–21], antireflection coatings [22], and magnetic mirrors [23], to name a few. So far, however, most metasurfaces are implemented for static operation and optimized for limited bandwidth of operation. To reach the next level of dynamic control over light, metasurfaces must include active and reconfigurable functionality that will drastically increase their potential and unlock a vast array of new application possibilities.

The fundamental challenge for achieving reconfigurable operation is to obtain large and continuous modulation of optical properties within subwavelength and low-Q meta-atom resonators [24, 25]. Desirable tuning mechanisms continuously shift the resonance frequency of the metastructure with at least one linewidth of maximal shift, thus enabling significant modulation of both amplitude and phase. These challenges have motivated several studies exploring different approaches, designs, and materials that provide extreme tunability. Previous investigations of active tuning in dielectric metasurfaces and meta-atoms have focused on ultrafast free-carrier injection [26–30]; coupling to liquid crystals [31, 32], to atomic vapor [33] or to epsilon-near zero materials [34, 35]; phase change materials [36, 37]; and MEMS [38–40]. However, none of these approaches provide a viable solution for a fully reconfigurable metadevice where at each subwavelength meta-atom, the phase and amplitude can be individually and continuously tuned to provide an arbitrary phase profile. Free-carrier approaches have shown only sub-linewidth resonance tuning, along with severe losses, as they require exceptionally high carrier generation rates. Phase change materials allow non-continuous switching

between two distinct states while coupling to background media, and MEMS-based approaches do not provide direct modulation of the resonator itself but rely on mechanical actuation or index modulation of substrates. Recent studies have showed that the thermo-optic effect (TOE), i.e. refractive index variation with temperature dn/dT can be used to induce large ($\Delta n \sim 1$) and continuous index shifts in materials having extraordinary thermal dependence [41, 42]. Recently, the TOE was also used to actively tune Si metasurfaces, but only at a limited temperature range (273–573 K) [43]. Here, we present a thorough study of the thermal tunability of Ge and Si meta-atoms and metasurfaces over a large temperature range 80–900 K. We demonstrate thermal tuning of Mie resonances due to the normal positive thermo-optic coefficient (TOC) ($dn/dT > 0$) over a wide infrared range. At higher temperatures and longer wavelengths, we show that thermal excitation of free carriers (FCs) becomes significant due to the bandgap shrinkage of the semiconductors, causing a reduction in dn/dT. With further increased temperatures, the sign of TOC is reversed ($dn/dT < 0$) culminating in a total negative induced index. We also demonstrate the tuning of high-order Mie resonances by several resonance linewidths with a temperature swing of $\Delta T < 100$ K. Finally, we exploit the larger TOC of Si at near-infrared (NIR) wavelengths for realizing amplitude modulators and tunable metafilters with Si metasurfaces.

Thermo-optic (TO) effects provide an ideal test bed for demonstrating and elucidating reconfigurable metasurface properties. TO tuning can provide large index shifts with no added losses and be integrated into electrically controlled architectures [44, 45]. Thus, TO tunability forms the basis for many reconfigurable integrated photonic devices [44–47]. However, the TOC of most materials is small for subwavelength applications; hence, typical TO applications exploit small index changes acting over distances much larger than a wavelength to achieve useful modulation. For efficient modulation of subwavelength resonators, the maximally induced index shift Δn should tune the resonance wavelength by more than its linewidth ($\Delta\lambda/\mathrm{FWHM} > 1$, where $\Delta\lambda$ is the resonance wavelength shift and FWHM is the full width at half max of the linewidth). The route for achieving this tunability is by maximizing the TOE using extraordinary materials [41, 42, 48, 49] and/or narrowing the resonance linewidth using high-Q modes [41], such as supported by asymmetric [32] or fano-resonant [10] metasurfaces or originating from bound states in the continuum [50]. Here, we study the TO tuning capabilities of Si and Ge – the most commonly used materials for dielectric metasurfaces and nanophotonics. The TO coefficients of these semiconductors are among the highest of natural materials [51], which, along with their high refractive indices and CMOS compatibility, makes them very attractive materials for reconfigurable metasurfaces. However, the typical TOC values ($\sim 1–5 \times 10^{-4}$ K^{-1}) requires large temperature modulation, which may cause problems if the TOC is strongly temperature dependent [41, 42]. In the mid-infrared (MIR) range; for instance, working at high temperatures can generate FC densities in semiconductors that dramatically alter the optical constants due to Dude-like dispersion. The total induced index shift of the semiconductor due to a positive temperature gradient is the sum of contributions from the normal TO effect and the thermal FC effect: $\Delta n = \Delta n_{TO} + \Delta n_{FC}$. In vast majority of materials, the TOC is positive; hence, $\Delta n_{TO} > 0$, while the FC term has a negative contribution $\Delta n_{FC} < 0$ (due to the plasma frequency blue shift caused by FCs, in a Drude model). The thermal FC term (Δn_{FC}) is particularly strong for low bandgap semiconductors with small effective masses [24, 41, 42] (Supporting Information), but in most semiconductors is negligible below ~500 K.

2 Results and discussion

The induced index shift of Si and Ge as a function of wavelength (2–16 μm) and temperature (80–850 K) is presented in Figure 1A and B. Refractive index shifts Δn are calculated with respect to index values at room temperature (RT). The index shifts in Si are almost wavelength independent for $\sim T < 700$ K, where the normal positive dn/dT is responsible for a near linear increase in Δn with temperature. For $T > 700$ K, Δn is wavelength dispersive since the density of thermally generated FCs is no longer negligible (Supporting Information Figures S1 and S2). Extracted dn/dT linecuts at different temperatures (Figure 1C) illustrate the temperature dependence and chromatic dispersion of dn/dT at various temperature regimes, specifically when dn/dT switches signs, i.e. $dn/dT < 0$, for $T = 800$ K (orange line). The strong dn/dT wavelength dispersion at 800 K (orange line) is due to a 15% decrease in bandgap, which generates an intrinsic FC density of $n_i \sim 10^{17}$ cm^{-3} (Supporting Information Figures S1 and S2) and associated negative Δn_{FC}. Thus, there is a point where both effects perfectly cancel out $\Delta n_{TO} = -\Delta n_{FC}$ and the total Δn is zero. In Ge, these thermal FC effects are further accentuated, as seen in Figure 1B and D. The smaller bandgap of Ge (0.66 eV at RT) compared to Si (1.12 eV at RT) and the lower FC effective mass cause a stronger FC contribution for the same temperature gradients. Therefore, FC effects play a significant role even at 500 K. For more elevated temperatures and longer wavelengths, FC effects

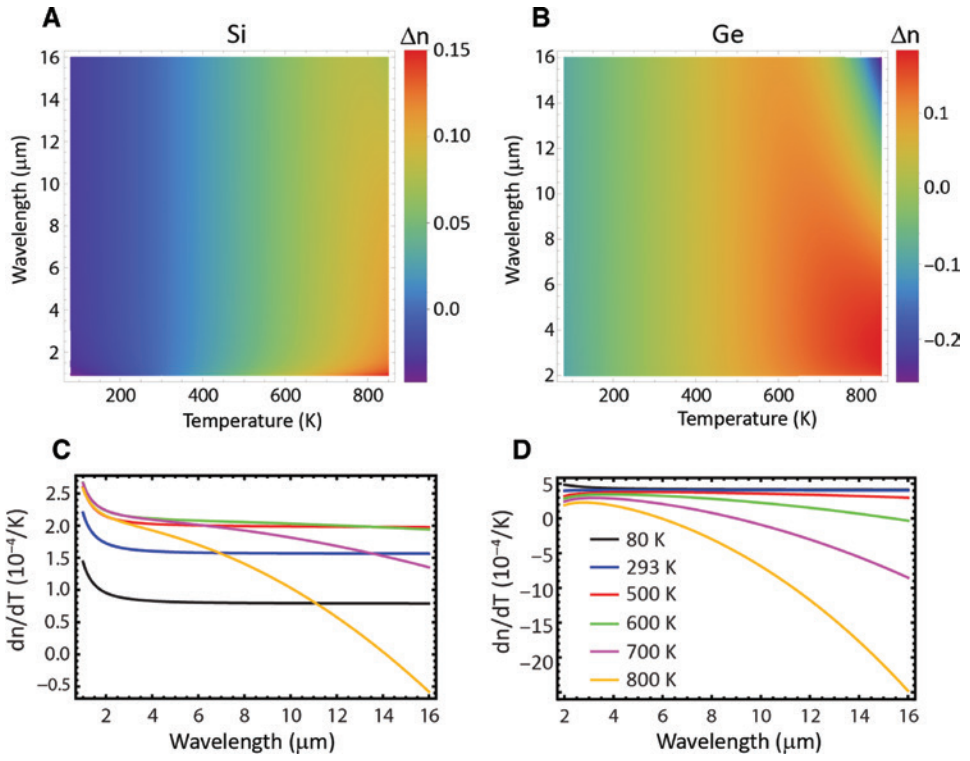

Figure 1: Temperature and wavelength dispersion of n and dn/dT in Silicon and Germanium.
Thermally induced index shifts in Si (A) and Ge (B) as a function of wavelength (2–16 μm) and temperature (80–850 K). (C) and (D) The chromatic dispersion of dn/dT at various temperatures in Si (C) and Ge (D). Each color plot corresponds to dn/dT at different temperatures as detailed in the legend of (D).

dominate over normal TO effects, leading to a negative and highly dispersive dn/dT at MIR and LWIR wavelengths. For example, at T = 800 K (orange line), dn/dT is almost an order of magnitude larger in magnitude at λ = 14 μm (-18×10^{-4} K^{-1}) compared to λ = 2 μm (2×10^{-4} K^{-1}).

To investigate thermal tunability capabilities, we study Si and Ge single spherical meta-atom resonators fabricated by laser ablation [24, 52]. Examples of Si (r = 1.9 μm) and Ge (r = 1.54 μm) meta-atom Mie resonators are illustrated in Figure 2A and B. A series of multipolar Mie resonances in the range 4–14 μm are observed using both analytical calculations (red dashed), FDTD simulations (red) and single particle infrared microspectroscopy (black). These multipolar resonances are labeled (see panels 2c and 2d) according to their polarization (magnetic or electric) and mode order (dipole, quadrupole, hexapole, etc.). The temperature-dependent spectra of these resonators (80–873 K for Si and 123–773 K for Ge, see experimental section for more details) are presented in Figure 2C and D. Spectral shifts are observed for all resonances as a response to the thermal modulation of the refractive index of the resonators.

When thermally generated FCs are negligible, all resonances are expected to red shift in response to a positive thermal gradient due to the normal positive dn/dT in both Si and Ge. This behavior is confirmed for both particles between cryogenic temperatures and up to 500 K. For more elevated temperatures, the shift in the long wavelength dipole modes deviates from the near-linear increase in wavelength. This behavior is more prominent in Ge due to its smaller bandgap and lighter effective mass (Supporting Information Section 1), which respectively facilitates higher FC concentrations at each given temperature and a larger index shift for a given carrier density. In Figure 2E and F, we track the temperature-dependent resonance wavelength shifts of the MD and ED, with respect to the RT resonance wavelength, and extract the corresponding index shifts Δn. Using our model for the temperature-dependent permittivity of the semiconductors (Supporting Information Section 1), we compare ex periments to calculated resonance and index shifts of the ED and MD modes (also see Figure S3, Supporting Information). For Si, the curvature of dn/dT significantly changes only above ~770 K and exclusively for the MD mode (due to its longer wavelength), as seen by the peak in both Δn and Δλ at ~800 K. Above the peak, the induced index and resonance wavelength decrease due to the generation of $n_i > 10^{17}$ cm^3 FCs; the sign of dn/dT has reversed

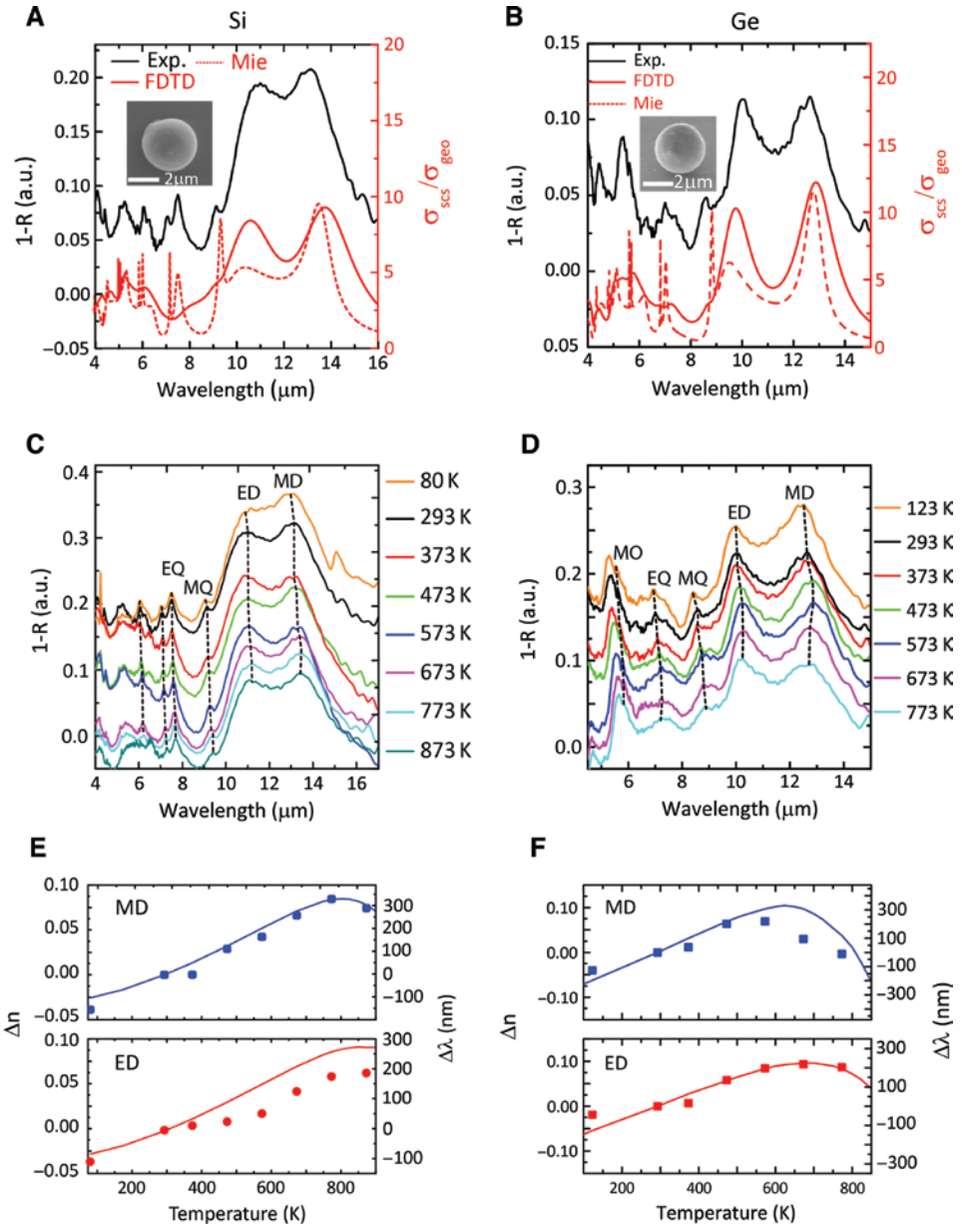

Figure 2: Thermal tunability in single semiconductor meta-atom resonators.
(A) and (B) Infrared spectra of Si (a, r = 1.9 μm) and Ge (b, r = 1.54 μm) spherical Mie resonators. Experimental spectra show good agreement with the calculated Mie scattering and FDTD cross-sections σ_{sca} normalized to the geometric cross-section σ_{geo}. A series of multipolar resonance peaks are visible in the spectra and correspond to dipole, quadrupole, hexapole, octapole, etc. (C) and (D) Temperature-dependent spectra of the spherical resonators between 80 K and 900 K. The spectral shifts of magnetic and electric dipole (MD and ED) and quadrupole (MQ and EQ) modes are highlighted. The dashed lines track the temperature-dependent resonance peaks and are a guide to the eye. The MO shift is also highlighted in the Ge resonator and is elaborated on in Figure 3. (E) and (F) The extracted induced index and resonance wavelength shifts as a function of temperature for MD and ED modes in Si (E) and Ge (F). Dots are experimentally extracted values, while solid lines are calculated shifts based on Mie theory.

$(dn/dT < 0)$ and now causes a slight blue shift for the MD mode (at this point, the curvature of the ED mode is also affected as it starts to flatten).

For the Ge resonator (Figure 2F), FC effects are more prominent and emerge at lower temperatures. Due to its smaller bandgap and lower effective masses, the dispersion of the induced index Δn of the MD mode starts to flatten at ~550 K, peaks at 600 K, then decreases at higher temperatures $(dn/dT < 0)$. For even more elevated temperatures, FCs dominate the index change, giving rise to a larger magnitude $|dn/dT|$. The behavior of the ED is similar, but the change in curvature of Δn is shifted to

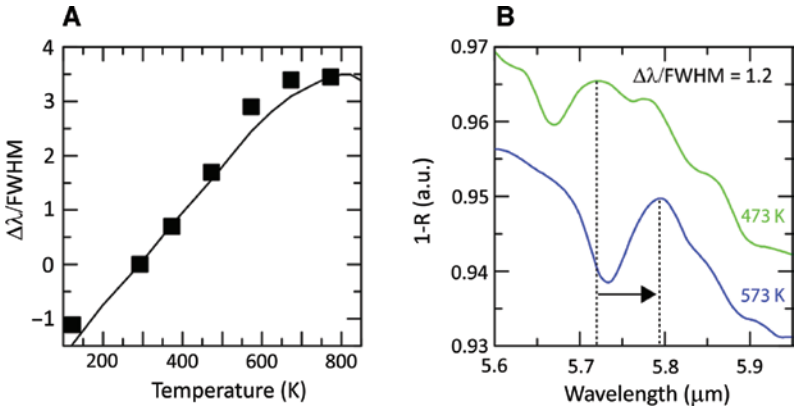

Figure 3: Normalized tunability (Δλ/FWHM) of high-order MO mode in the Ge resonator.
(A) Temperature-dependent MO shifts normalized to the resonance linewidth. (B) Tuning by more than one resonance linewidth (Δλ/FWHM = 1.2) with a ΔT = 100 K temperature gradient.

higher temperature T ~ 675 K since the FC effect is smaller at shorter wavelengths. Altogether, these results show that the dispersion, the sign, and magnitude of dn/dT can be controlled with temperature in low and moderate bandgap semiconductor resonators through the generation of FCs. This can be used to engineer the dispersion of dn/dT and for tuning of infrared meta-atoms and resonators.

The ability to maximize the control over the phase and amplitude of incident light depends on the capability of tuning resonance wavelengths by more than one linewidth Δλ/FWHM > 1. Figure 3 presents the normalized tunability (Δλ/FWHM) of a high-order magnetic octapole (MO) mode that is tuned by ~4.5 normalized linewidths across the 123–773 K temperature range. This wide normalized tunability becomes possible due to an order of magnitude increase in the resonance Q-factor of $Q_{MO} = 88.1$ compared with $Q_{MD} = 8.2$ for the MD mode. As evident from Figure 3A, the normalized tunability exhibits a linear like dependence up to 675 K, with almost one normalized linewidth per 100 K. For ~T > 675 K, the linear dependence breaks as FC effects become significant, which leads to a rapid saturation of tunability with increased temperature. Figure 3B presents the spectral shift of Δλ/FWHM = 1.2 with a temperature gradient of ΔT = 100 K. Such tunability with a practical temperature difference of ΔT = 100 K would be useful for implementing reconfigurable high-Q Ge metasurfaces.

A different route for increasing the TO normalized tunability is to exploit the larger TOC at shorter wavelengths in the vicinity of the material bandgap. As seen in Figure 1C, the dn/dT values are up to 50% larger in Si around 1 μm. Below, we demonstrate thermally reconfigurable metasurfaces in the NIR range using a Si disk array on SiO_2 substrate. Figure 4A shows experimental and FDTD reflection spectra of a silicon disk array with disk diameter and height of d = 290 nm and h = 280 nm, respectively, and periodicity a = 590 nm. Both experimental and FDTD spectra show pronounced MD and ED resonances (Q ~ 21) at λ = 1.12 μm and λ = 0.95 μm, respectively. The experimental temperature dependence of these resonances is presented in Figure 4B (the spectra are vertically shifted along the y-axis for visibility), where both dipole modes are continuously red shifted with increasing temperatures. The extracted index and resonance wavelength shifts Δn and Δλ are presented in Figure 4C for both dipole modes (Δn and Δλ are calculated with respect to index and resonance wavelengths values at RT). The higher TOC at shorter wavelengths is evinced by a larger induced index shift Δn for the ED mode compared to the MD mode. Extracted dn/dT values for both MD and ED modes are similar or slightly higher than reported values [51]. These high dn/dT values at the ED resonance wavelengths, combined with relatively narrow linewidths (Q ~ 21), allows for tunable metafilter operation (Figure 4D) with amplitude modulation of more than 95% (13 dB) for ΔT = 380 K at λ = 950 nm [60% (4 dB) amplitude modulation for ΔT = 280 K]. Further reduction in the required temperature modulation may be achieved by engineering ultrahigh-Q metasurfaces (such as the high-order Mie resonance presented in Figure 3) that enable normalized tunability Δλ/FWHM > 1 with temperature modulation of tens of kelvin or less [32, 41]. Importantly, thermal tunability in Si metasurfaces can be extended to the visible range, with improved performance due to the expected increase of dn/dT at shorter wavelengths. Also, thermal tuning can be implemented using electrically controlled architectures with independent control for each element [45, 48].

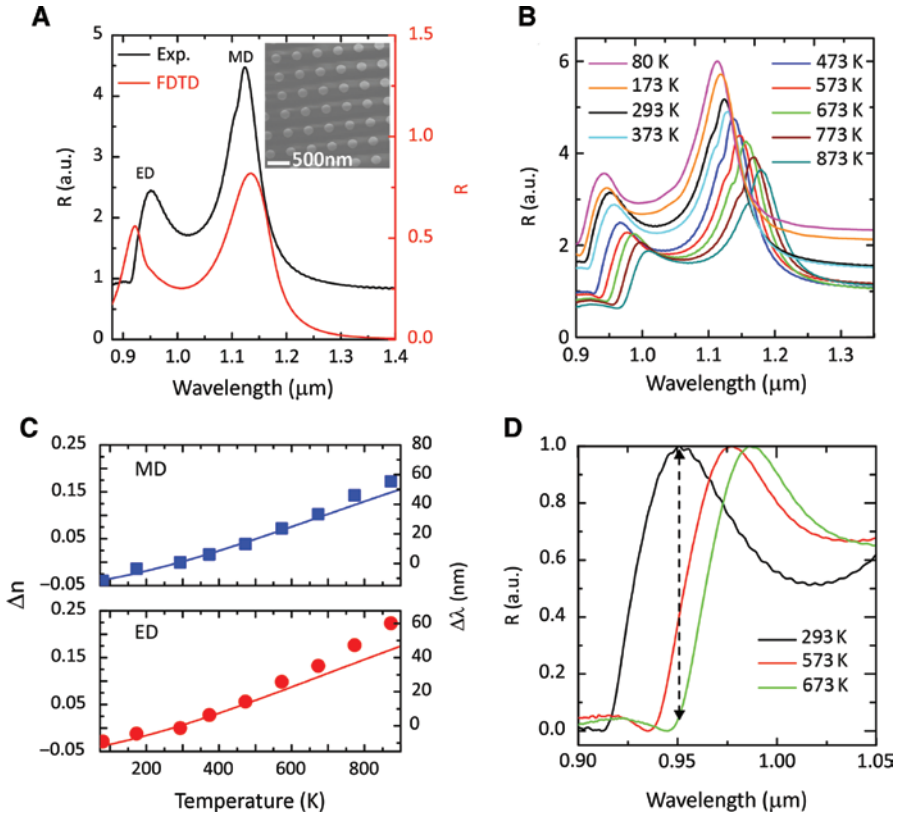

Figure 4: Thermally reconfigurable Si metasurfaces.
(A) RT NIR reflection spectra of a Si metasurface disk array with disk diameter and height of d = 290 nm and h = 280 nm, respectively, and periodicity a = 590 nm on a SiO2 substrate. Experimentally measured (black) and FDTD (red) spectra are in good match showing the fundamental MD and ED modes. The inset presents an SEM image of the metasurface. (B) Temperature-dependent spectra exhibiting continuously red-shifted MD and ED resonances with increasing temperature. The spectra are vertically shifted along the y-axis for visibility. (C) Thermally induced index and wavelength shifts of MD and ED modes. (D) Thermally reconfigurable metafilter demonstration, exhibiting 4 dB and 13 dB amplitude modulation when a temperature gradient of $\Delta T = 280$ K and $\Delta T = 380$ K is applied, respectively.

3 Conclusions

In summary, we studied the thermal tuning capabilities of Si and Ge single resonators and metasurfaces over the large temperature range 80–873 K. We demonstrated temperature-dependent resonance frequency shifts that follow a modified model of the traditional TOE that takes into account effects of thermally generated FCs. We showed that at low and intermediate temperatures, all resonances red-shift according to the normal positive dispersion of TOC ($dn/dT > 0$). At higher temperatures and longer wavelengths, however, thermally generated FCs contribute a negative component to the total TOC and can reverse its sign, i.e. yielding a $dn/dT < 0$. This dispersion anomaly is evinced by a continuous change in the resonance shift from red- to blue-shift. We also demonstrated more than a unit of normalized tunability $\Delta\lambda/FWHM = 1.2$ of high-order octapole modes in Ge resonators with a temperature gradient of $\Delta T < 100$ K. Ultimately, we exploit the larger TOC at short NIR wavelengths in Si to demonstrate thermally reconfigurable metasurface functionality such as amplitude modulators and tunable metafilters. This work highlights the opportunities and potential of thermally tunable semiconductor metasurfaces and can pave the way to efficient high-Q reconfigurable metadevices.

4 Methods

4.1 Sample fabrication

Si and Ge spherical resonators were fabricated by femtosecond laser ablation. In these experiments, we used a commercial femtosecond laser system (Spitfire, Spectra Physics) delivering ~1 mJ pulses with ~120 fs duration with central wavelength of 800 nm and variable repetition rate. Pulse energies ranging between 20 and 200 μJ at 20 Hz repetition rate were used in ablation experiments.

More details on ablation experiments can be found in previous works [24, 52].

Si metasurfaces were fabricated per a previously reported procedure [53]: amorphous silicon was deposited onto fused quartz substrates with an Advanced Vacuum PECVD. Patterning was done using ultraviolet photolithography and deep reactive-ion-etching process using a PlasmaTherm 770 SLR system.

4.2 Optical characterization

Single particle spectroscopy at various temperatures was conducted using an FTIR (Vertex 70, Bruker) coupled to an infrared microscope (Hyperion 3000, Bruker) using a thermal stage (THMS600, Linkam). More details on single particle spectroscopy were reported elsewhere [24]. Finite difference time domain (FDTD) calculations were performed using the Lumerical Solutions FDTD Solver, Version 8.7.3. A non-uniformal conformal mesh was used. A mesh size at least 10× smaller than the minimum wavelength in the material was used with boundary conditions of perfectly matched layers.

Acknowledgments: This work was supported by the Air Force Office of Scientific Research, Funder Id: http://dx.doi.org/10.13039/100006831 (FA9550-16-1-0393) and by the UC Office of the President Multi-campus Research Programs and Initiatives (MR-15-328528). Microscopy was performed with support from MRSEC Program of the NSF under award no. DMR 1121053, a member of the NSF-funded Materials Research Facilities Network. Numerical calculations were performed with the support from the Centre for Scientific Computing from the CNSI, MRL: an NSF MRSEC (DMR-1121053), NSF CNS-0960316. N.A.B. acknowledges support from the Department of Defense NDSEG fellowship.

Conflicts of interest: There are no conflicts to declare.

References

[1] Yu NF, Genevet P, Kats MA, et al. Light propagation with phase discontinuities: generalized laws of reflection and refraction. Science 2011;334:333–7.
[2] Jahani S, Jacob Z. All-dielectric metamaterials. Nat Nanotechnol 2016;11:23–6.
[3] Kuznetsov AI, Miroshnichenko AE, Brongersma ML, Kivshar YS, Luk'yanchuk B. Optically resonant dielectric nanostructures. Science 2016;354. doi:10.1126/science.aag2472-1-2472-8.
[4] Arbabi A, Horie Y, Bagheri M, Faraon A. Dielectric metasurfaces for complete control of phase and polarization with subwavelength spatial resolution and high transmission. Nat Nanotechnol 2015;10:937–43.
[5] Aieta F, Kats MA, Genevet P, Capasso F. Applied optics. Multiwavelength achromatic metasurfaces by dispersive phase compensation. Science 2015;347:1342–5.
[6] Khorasaninejad M, Chen WT, Devlin RC, Oh J, Zhu AY, Capasso F. Metalenses at visible wavelengths: diffraction-limited focusing and subwavelength resolution imaging. Science 2016;352:1190–4.
[7] Arbabi E, Arbabi A, Kamali SM, Horie Y, Faraon A. Controlling the sign of chromatic dispersion in diffractive optics with dielectric metasurfaces. Optica 2017;4:625–32.
[8] Lin DM, Fan PY, Hasman E, Brongersma ML. Dielectric gradient metasurface optical elements. Science 2014;345:298–302.
[9] Yuan GH, Rogers ETF, Zheludev NI. Achromatic super-oscillatory lenses with sub-wavelength focusing. Light-Sci Appl 2017;6:e17036.
[10] Yang YM, Wang W, Boulesbaa A, et al. Nonlinear fano-resonant dielectric metasurfaces. Nano Lett 2015;15:7388–93.
[11] Smirnova D, Kivshar YS. Multipolar nonlinear nanophotonics. Optica 2016;3:1241–55.
[12] Liu S, Sinclair MB, Saravi S, et al. Resonantly enhanced second-harmonic generation using III–V semiconductor all-dielectric metasurfaces. Nano Lett 2016;16:5426–32.
[13] Sell D, Yang JJ, Doshay S, Zhang K, Fan JA. Visible light metasurfaces based on single-crystal silicon. ACS Photonics 2016;3:1919–25.
[14] Arbabi A, Arbabi E, Horie Y, Kamali SM, Faraon A. Planar metasurface retroreflector. Nat Photonics 2017;11:415–20.
[15] Chong KE, Staude I, James A, et al. Polarization-independent silicon metadevices for efficient optical wavefront control. Nano Lett 2015;15:5369–74.
[16] Decker M, Staude I, Falkner M, et al. High-efficiency dielectric Huygens' surfaces. Adv Opt Mater 2015;3:813–20.
[17] Yang YM, Wang W, Moitra P, Kravchenko II, Briggs DP, Valentine J. Dielectric meta-reflectarray for broadband linear polarization conversion and optical vortex generation. Nano Lett 2014;14:1394–9.
[18] Shalaev MI, Sun J, Tsukernik A, Pandey A, Nikolskiy K, Litchinitser NM. High-efficiency all-dielectric metasurfaces for ultracompact beam manipulation in transmission mode. Nano Lett 2015;15:6261–6.
[19] Devlin RC, Khorasaninejad M, Chen WT, Oh J, Capasso F. Broadband high-efficiency dielectric metasurfaces for the visible spectrum. Proc Natl Acad Sci USA 2016;113:10473–8.
[20] Li Z, Kim I, Zhang L, et al. Dielectric meta-holograms enabled with dual magnetic resonances in visible light. ACS Nano 2017;11:9382–9.
[21] Xie Z, Lei T, Si G, et al. Meta-holograms with full parameter control of wavefront over a 1000 nm bandwidth. ACS Photonics 2017;4:2158–64.
[22] Spinelli P, Verschuuren MA, Polman A. Broadband omnidirectional antireflection coating based on subwavelength surface Mie resonators. Nat Commun 2012;3:692.
[23] Liu S, Sinclair MB, Mahony TS, et al. Optical magnetic mirrors without metals. Optica 2014;1:250–6.

[24] Lewi T, Iyer PP, Butakov NA, Mikhailovsky AA, Schuller JA. Widely tunable infrared antennas using free carrier refraction. Nano Lett 2015;15:8188–93.
[25] Iyer PP, Pendharkar M, Schuller JA. Electrically reconfigurable metasurfaces using heterojunction resonators. Adv Opt Mater 2016;4:1582–8.
[26] Makarov S, Kudryashov S, Mukhin I, et al. Tuning of magnetic optical response in a dielectric nanoparticle by ultrafast photoexcitation of dense electron-hole plasma. Nano Lett 2015;15:6187–92.
[27] Shcherbakov MR, Vabishchevich PP, Shorokhov AS, et al. Ultrafast all-optical switching with magnetic resonances in nonlinear dielectric nanostructures. Nano Lett 2015;15:6985–90.
[28] Baranov DG, Makarov SV, Milichko VA, Kudryashov SI, Krasnok AE, Belov PA. Nonlinear transient dynamics of photoexcited resonant silicon nanostructures. ACS Photonics 2016;3:1546–51.
[29] Fischer MP, Schmidt C, Sakat E, et al. Optical activation of germanium plasmonic antennas in the mid-infrared. Phys Rev Lett 2016;117:047401.
[30] Shcherbakov MR, Liu S, Zubyuk VV, et al. Ultrafast all-optical tuning of direct-gap semiconductor metasurfaces. Nat Commun 2017;8:17.
[31] Sautter J, Staude I, Decker M, et al. Active tuning of all-dielectric metasurfaces. ACS Nano 2015;9:4308–15.
[32] Parry M, Komar A, Hopkins B, et al. Active tuning of high-Q dielectric metasurfaces. Appl Phys Lett 2017;111:053102.
[33] Bar-David J, Stern L, Levy U. Dynamic control over the optical transmission of nanoscale dielectric metasurface by alkali vapors. Nano Lett 2017;17:1127–31.
[34] Forouzmand A, Salary MM, Inampudi S, Mosallaei H. A tunable multigate indium-tin-oxide-assisted all-dielectric metasurface. Adv Opt Mater 2018;6. doi:Artn 1701275 10.1002/Adom.201701275:1–13.
[35] Howes A, Wang WY, Kravchenko I, Valentine J. Dynamic transmission control based on all-dielectric Huygens metasurfaces. Optica 2018;5:787–92.
[36] Wang Q, Rogers ETF, Gholipour B, et al. Optically reconfigurable metasurfaces and photonic devices based on phase change materials. Nat Photon 2016;10:60–5.
[37] Karvounis A, Gholipour B, MacDonald KF, Zheludev NI. All-dielectric phase-change reconfigurable metasurface. Appl Phys Lett 2016;109:051103.
[38] Kamali SM, Arbabi E, Arbabi A, Horie Y, Faraon A. Highly tunable elastic dielectric metasurface lenses. Laser Photonics Rev 2016;10:1002–8.
[39] Arbabi E, Arbabi A, Kamali SM, Horie Y, Faraji-Dana MS, Faraon A. MEMS-tunable dielectric metasurface lens. Nat Commun 2018;9:812.
[40] She A, Zhang S, Shian S, Clarke DR, Capasso F. Adaptive metalenses with simultaneous electrical control of focal length, astigmatism, and shift. Sci Adv 2018;4. doi:10.1126/sciadv.aap9957-1-9957-7.
[41] Lewi T, Evans HA, Butakov NA, Schuller JA. Ultrawide thermo-optic tuning of PbTe meta-atoms. Nano Lett 2017;17:3940–5.
[42] Iyer PP, Pendharkar M, Palmstrøm CJ, Schuller JA. Ultrawide thermal free-carrier tuning of dielectric antennas coupled to epsilon-near-zero substrates. Nat Commun 2017;8:472.
[43] Rahmani M, Xu L, Miroshnichenko AE, et al. Reversible thermal tuning of all-dielectric metasurfaces. Adv Funct Mater 2017;27. doi:10.1002/adfm.201700580-1-7.
[44] Padmaraju K, Chan J, Chen L, Lipson M, Bergman K. Thermal stabilization of a microring modulator using feedback control. Opt Express 2012;20:27999–8008.
[45] Sun J, Timurdogan E, Yaacobi A, Hosseini ES, Watts MR. Large-scale nanophotonic phased array. Nature 2013;493:195–9.
[46] Hulme JC, Doylend JK, Heck MJR, et al. Fully integrated hybrid silicon two dimensional beam scanner. Opt Express 2015;23:5861–74.
[47] Lee BS, Zhang M, Barbosa FAS, et al. On-chip thermo-optic tuning of suspended microresonators. Opt Express 2017;25:12109–20.
[48] Butakov NA, Knight MW, Lewi T, et al. Broadband electrically tunable dielectric resonators using metal-insulator transitions. ACS Photonics 2018;5:4056–60.
[49] Iyer PP, DeCrescent RA, Lewi T, Antonellis N, Schuller JA. Uniform thermo-optic tunability of dielectric metalenses. Phys Rev Appl 2018;10:044029.
[50] Koshelev K, Lepeshov S, Liu M, Bogdanov A, Kivshar Y. Asymmetric metasurfaces with high-Q resonances governed by bound states in the continuum. Phys Rev Lett 2018;121:193903.
[51] Ghosh G. Handbook of optical constants of solids: handbook of thermo-optic coefficients of optical materials with applications. USA, Academic Press, 1998.
[52] Butakov NA, Valmianski I, Lewi T, et al. Switchable plasmonic–dielectric resonators with metal-insulator transitions. ACS Photonics 2017;5:371–7.
[53] Butakov NA, Schuller JA. Designing multipolar resonances in dielectric metamaterials. Sci Rep 2016;6:38487.

Supplementary Material: The online version of this article offers supplementary material (https://doi.org/10.1515/nanoph-2018-0178).